FLUID-ELASTIC INSTABILITY OF ROTATED SQUARE TUBE ARRAY IN AN AIR-WATER TWO-PHASE CROSS-FLOW

HEUNG JUNE CHUNG* and IN-CHEOL CHU
Korea Atomic Energy Research Institute
150 Deokjin-dong, Yuseong, Daejeon, Korea 305-353
*Corresponding author. E-mail : hjchung@kaeri.re.kr

Received June 9, 2005
Accepted for Publication December 20, 2005

Fluid-elastic instability in an air-water two-phase cross-flow has been experimentally investigated using two different arrays of straight tube bundles: normal square (NS) array and rotated square (RS) array tube bundles with the same pitch-to-diameter ratio of 1.633. Experiments have been performed over wide ranges of mass flux and void fraction. The quantitative tube vibration displacement was measured using a pair of strain gages and the detailed orbit of the tube motion was analyzed from high-speed video recordings. The present study provides the flow pattern, detailed tube vibration response, damping ratio, hydrodynamic mass, and the fluid-elastic instability for each tube bundle. Tube vibration characteristics of the RS array tube bundle in the two-phase flow condition were quite different from those of the NS array tube bundle with respect to the vortex shedding induced vibration and the shape of the oval orbit of the tube motion at the fluid-elastic instability as well as the fluid-elastic instability constant.

KEYWORDS : Fluid-elastic Instability, Flow-induced Vibration, Damping Ratio, Hydrodynamic Mass, Two-phase Cross-flow, Normal Square Array, Rotated Square Array

1. INTRODUCTION

The U-bend region of a nuclear steam generator and many tube-and-shell heat exchangers which undergo a high velocity two-phase cross-flow are highly susceptible to flow-induced vibration. In various flow-induced vibration mechanisms, it is generally known that fluid-elastic instability is the most common(?) cause of short-term tube failure.

Since the mid-1980s, numerous experimental studies have been carried out to investigate the fluid-elastic instability for various configurations of tube bundles in two-phase cross-flows [1~11]. Among a number of comprehensive studies, considerable progress in particular has been made by Pettigrew et al. [1~4].

One of the most important findings is that above a certain void fraction, the critical flow velocity for the fluid-elastic instability becomes much lower than the value predicted by the typical Connors' equation. (Who? Pettigrew et al??) explained that this phenomenon is likely due to the flow regime transition from a bubbly flow to an intermittent flow.

While their finding has a significant effect on the design of heat exchangers and nuclear steam generators, it was not experimentally validated or confirmed until recently. Chu et al. [11] recently performed supplementary experiments to validate the findings of Pettigrew et al. using a rotated triangular array tube bundle with a pitch-to-diameter ratio (p/d) of 1.47. Not only did they obtain a similar fluid-elastic instability constant (K) for Connors' equation with that of Pettigrew et al., but they also confirmed the transition of the fluid-elastic instability region and its close relationship with the flow regime transition.

In addition, most of the previous experiments were performed using triangular tube bundles or normal square arrays with a p/d ratio below 1.5. According to Pettigrew et al. [3], the fluid-elastic instability constant (K) varies according to the array type and the p/d ratio of the tube bundle.

Therefore, for tube bundles with a p/d above 1.5, there is an insufficient experimental database for the fluid-elastic instability in two-phase cross-flows, especially in the case of rotated square array tube bundles.

The main objectives of the present study are to investigate the flow-induced vibration characteristics in normal square (NS) array and rotated square (RS) array tube bundles with a p/d of 1.633, and to broaden the experimental database for the fluid-elastic instability in a two-phase cross-flow.

2. EXPERIMENTAL METHOD

Figure 1 shows a schematic of the present test facility, which consists of a test section, water supply system, air supply system, and a measurement and control system.

The test section has a cross-sectional dimension of 88 × 600 mm. As working fluids, air and water of atmospheric pressure and room temperature are injected into the bottom part of the test section. Cantilevered straight tube bundles were installed in a rectangular flow channel about 1000 mm downstream of the air and water injection point. A two-phase flow distributor and a honeycomb were installed upstream of the tube bundle to provide a uniform and homogeneous two-phase cross-flow.

The water pump has a capacity of 100 m3/hr at a 50 m water head, and the air blower has a capacity of 6.5 m^3/min at a discharge pressure of 2.6 bar. The water and air injection flow rate are finely controlled by VVVF inverters.

Fluid-elastic instability characteristics have been experimentally investigated using two different tube bundles, i.e. NS array and RS array tube bundles with a p/d of 1.633, as shown in Fig. 2. Each tube bundle was assembled with a brass tube having a length of 600 mm, diameter of 12.7 mm, and thickness of 0.89 mm. The first mode natural frequency of the tube in air was measured using a miniature 3-axis accelerometer. The tube natural frequencies for NS and RS arrays are 21.44 Hz and 21.49 Hz, respectively.

As shown in Fig. 2, half-cylinder tubes made of acryl were installed on both side walls of the flow channel so as to minimize the non-uniformity in the flow distribution due to the wall effect. In addition, two different arrays of dummy tube bundles were installed just upstream of each cantilevered tube bundle to provide a more stable two-phase flow in each cantilevered tube bundle. Both ends of the tubes in the dummy bundle were tightly fixed.

In order to visually observe and obtain high speed video recordings of the flow pattern and tube vibration motions, transparent windows were installed at both side walls and the tube end wall (the opposite to the cantilevered side).

Each installed tube can vibrate in a cantilevered mode (flexible tube) or in a both sides clamped mode (rigid tube). A tube bundle with all flexible tubes (flexible tube bundle) was used for the tests to find the onset of the fluid-elastic instability, and a tube bundle with a single flexible tube surrounded by rigid tubes (rigid tube bundle) was used for the tests to measure the damping ratio and the hydrodynamic mass.

The tube vibration responses of the single flexible tube in the drag and the lift directions were measured with a pair of orthogonally installed strain gages. The output voltage of each strain gage was carefully calibrated against the exactly known values of the tube displacement. Thus, the

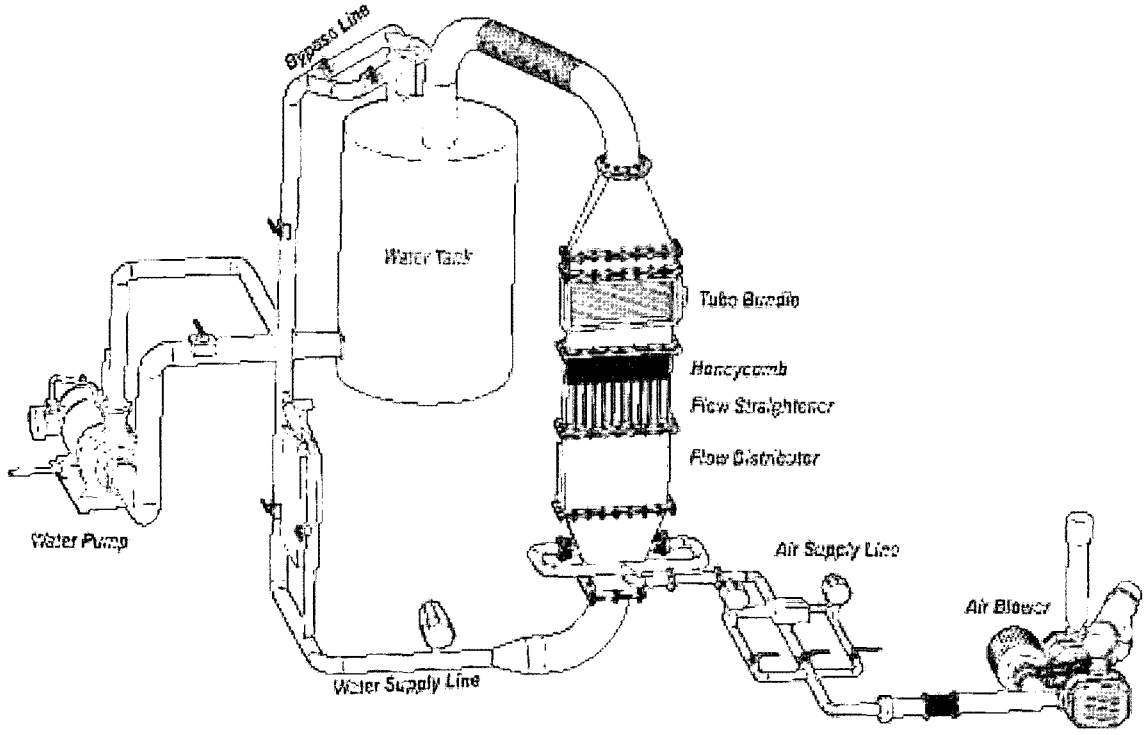

Fig. 1. Schematic Diagram of the Test Loop

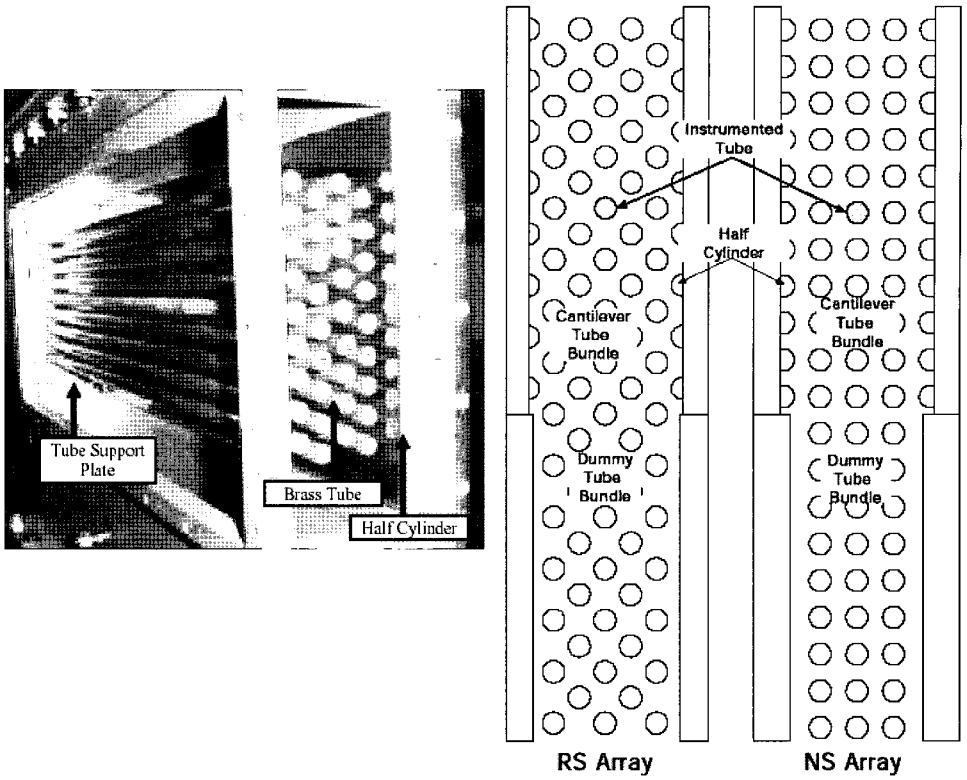

Fig. 2. Test Section and Tube Bundle Configuration

actual tube displacement could be directly evaluated from the voltage output of the strain gage.

In order to be consistent with the existing experimental results, all the two-phase flow parameters such as the void fraction, density, and velocity were taken as homogeneous flow parameters. The void fraction and the two-phase density are defined as follows:

$$\alpha = \frac{Q_g}{Q_l + Q_g} \tag{1}$$

$$\rho = \alpha \cdot \rho_g + (1-\alpha) \cdot \rho_l \tag{2}$$

The freestream velocity is defined as follows:

$$V_\infty = \frac{Q_l + Q_g}{A_\infty} \tag{3}$$

Regardless of the tube bundle arrays, the gap velocity is defined as

$$V_g = V_\infty \frac{p}{(p-d)} \tag{4}$$

Experiments to determine the onset condition of fluid -elastic instability have been performed separately from experiments to measure the damping and the hydrodynamic mass.

For the fluid-elastic instability tests, the homogeneous two-phase gap velocity was increased until the tube vibration amplitudes were high enough to indicate fluid-elastic instability while maintaining the homogeneous void fraction constant for each flow rate. The flow rate was increased in sufficiently small steps to clearly distinguish the onset of instability.

Damping and hydrodynamic mass were measured simultaneously at sufficiently low mass flux conditions for given void fractions. Power spectral density function (PSD) was evaluated from the time domain tube vibration waveform, which had been measured for 1,800 seconds. From this PSD function, the natural frequency of the tube, total damping ratio, and hydrodynamic mass were calculated. The sampling rate for the measurement of the time domain waveform was 100 Hz.

Finally, the fluid-elastic instability constant (K) and the exponent (n) of the mass damping ratio were determined using these parameters.

3. EXPERIMENTAL RESULTS

3.1 Flow Pattern

Flow patterns were identified from a visual observation and high speed video recordings through the transparent windows at the free vibrating tube end and side walls. A bubbly flow was observed below a homogeneous void fraction of approximately 80%, and the flow regime transition to an intermittent flow occurred when the void fraction was above 90%. In addition, the flow regime transition was observed at a void fraction of 90% regardless of the tube bundle arrays.

Figure 3 shows a comparison of the present data with the flow regime map of Ulbrich and Mewes [11]. They developed the flow regime map for a horizontal tube bundle under an air-water two-phase cross-flow condition, where the tubes were arranged in a normal square array with a p/d of 1.5 and the tube diameter was 20 mm.

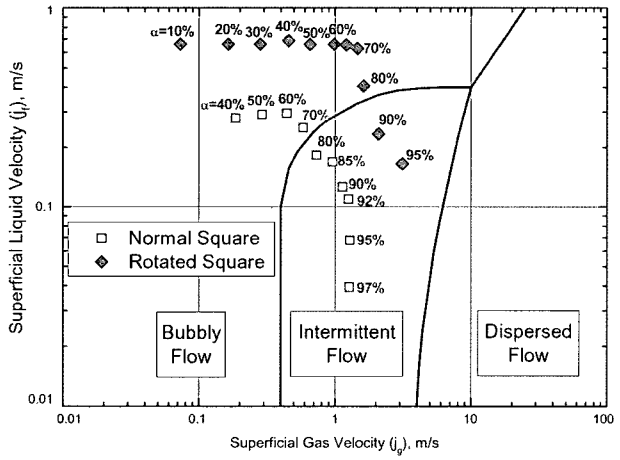

Fig. 3. Flow Regime Map

The flow velocities between a 60 ~ 70 % void fraction were obtained at the onset of the fluid-elastic instability. In other void fraction conditions, the present data corresponds to the maximum flow velocities that could be attained by the present experimental facility. The flow regime transition from bubbly flow to an intermittent flow was predicted to occur at a void fraction of 70 ~ 80 % for the NS array tube bundle and at a void fraction of 80 ~ 90 % for the RS array tube bundle, respectively. Although the predicted flow regime transition criteria were similar to the present experimental results, the existing database still suffers from a lack of experimental data for various tube bundle configurations.

3.2 Tube Vibration Response

The root-mean-square (RMS) tube displacements in the NS array tube bundle under a two-phase cross-flow are shown in Fig. 4. Experiments were performed using a flexible tube bundle for a void fraction condition between 40 and 97 %.

When the homogeneous gap velocity was low, tube vibration responses showed turbulence-induced excitation vibration characteristics. The tube vibration amplitude was similar both in the drag and the lift directions or slightly larger in the drag direction, and the increasing rate of the RMS tube displacement with the gap velocity was not significant.

Above a certain gap velocity, the RMS tube displacement showed a sharp increase with respect to a small

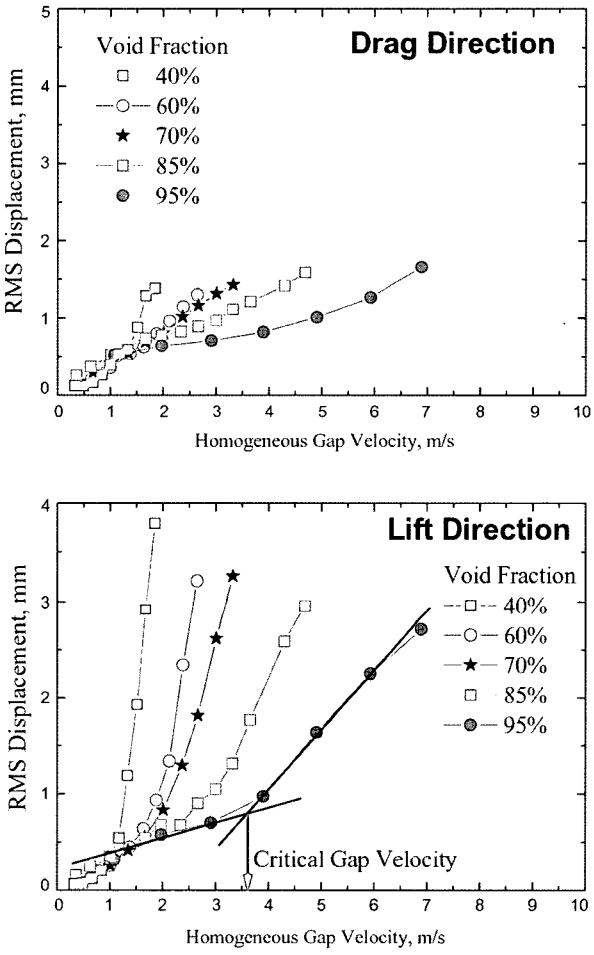

Fig. 4. RMS Tube Displacement in the NS Array Tube Bundle

increase in the gap velocity, which can be defined as the critical gap velocity of the fluid-elastic instability. As shown in Fig. 4, the critical gap velocity is determined at the intersection of two slopes corresponding to the turbulent excitation region and the fluid-elastic instability region, respectively.

In the case of the NS array tube bundle, a sharp increase of the tube displacement or fluid-elastic instability was observed in the lift direction for all void fraction conditions. That is, as generally recognized in previous studies, the lift directional tube vibration motion was dominant over the drag directional motion at the fluid-elastic instability condition.

Figures 5 and 6 show the tube vibration response of the RS array tube bundle for a void fraction of 10 ~ 50 % and 60 ~ 95%, respectively. In Fig. 5, it can be clearly seen that the vortex shedding vibration resonance occurred up to a high void fraction of 50 %. In addition, the tube vibration motion was dominant in the lift direction over the drag direction.

Taylor et al. [5] noted that beyond a 15 % void fraction no evidence of a periodic wake or a vortex shedding could be found in the vibration response spectra. Their tube bundle had a NS array with a diameter of 12.7mm and a p/d of 1.47. Also, Feenstra et al. [10] deduced that a small amount of vapor (5 ~ 10 % of void fraction) was sufficient to disrupt the vortex shedding excitation of the tube bundle. They used a small scale normal square array tube bundle with a tube diameter of 7.11 mm and a p/d of 1.485. However, Chu et al. [11] did not observe the vortex shedding vibration at a void fraction of 40 % for their rotated triangular array tube bundle with a p/d of 1.47. In the present NS array tube bundle tests, the vortex shedding vibration did not occur at a void fraction of 40 %.

However, it has been observed in the present study that a vortex shedding vibration excitation can occur up to a void fraction of 50 % in the case of a RS array tube bundle with a tube diameter of 12.7 mm and a p/d of 1.633. The

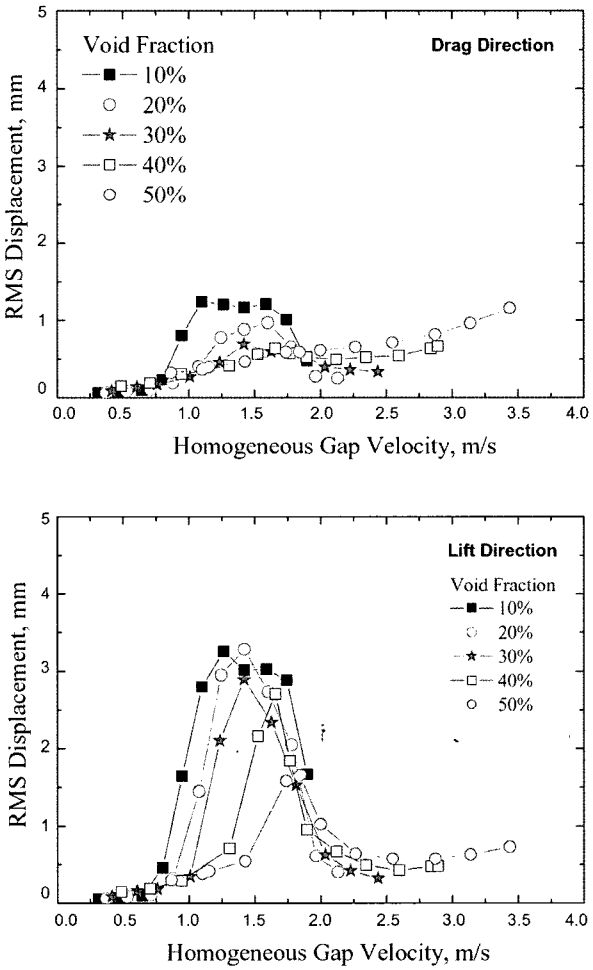

Fig. 5. RMS Tube Displacement in the RS Array Tube Bundle (void fraction of 10 ~ 50 %)

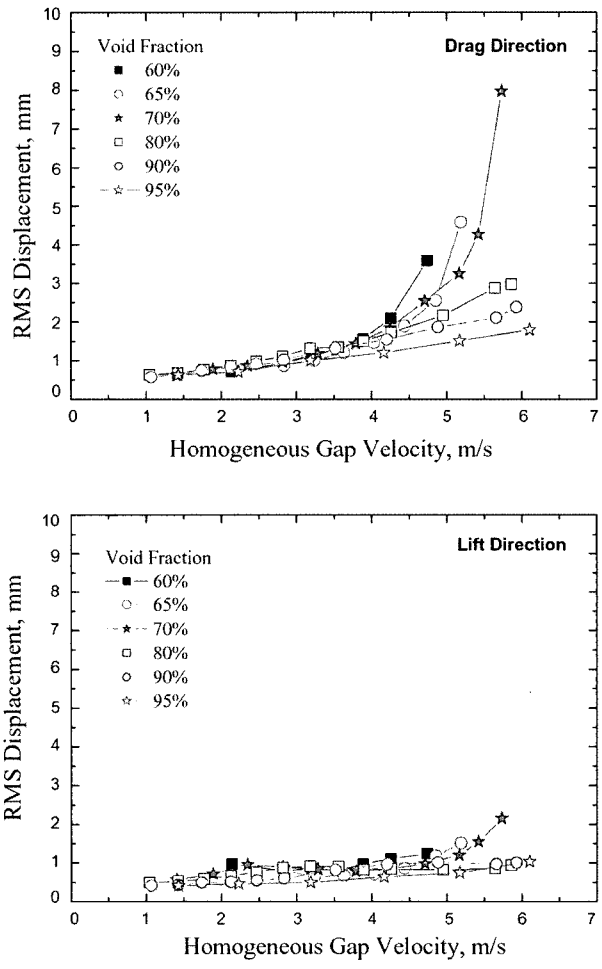

Fig. 6. RMS Tube Displacement in the RS Array Tube Bundle (void fraction of 60 ~ 95 %)

Strouhal number is defined as given by Eq. (5), and has a range of 0.15 ~ 0.19 with respect to the homogeneous void fraction.

$$St = \frac{fD}{V_g} \tag{5}$$

Due to the limited capacity of the water pump, the onset of the fluid-elastic instability condition was not reached. However, as can be seen in Figs. 4 and 5, the maximum gap velocities supplied in the present RS array tests were much higher than the critical gap velocities of the present NS array tests for very similar void fractions. For example, the maximum gap velocities of the RS array were 2.89 and 3.44 m/s for the void fractions of 40 % and 50 %, respectively. On the other hand, the critical gap velocities of the NS array were 1.2 and 1.5 m/s for the void fractions of 40 % and 50 %, respectively.

When the void fraction was higher than 60 %, vortex shedding vibration excitation could no longer be observed from the tube vibration response in the RS array.

In the case of void fractions of 60 ~ 70 % in the RS array, as shown in Fig. 6, the onset of fluid-elastic instability was observed in the drag directional tube vibration response but not in the lift directional tube response. This isa different finding from the general postulation that the tube vibration motion should be dominant in the lift direction over the

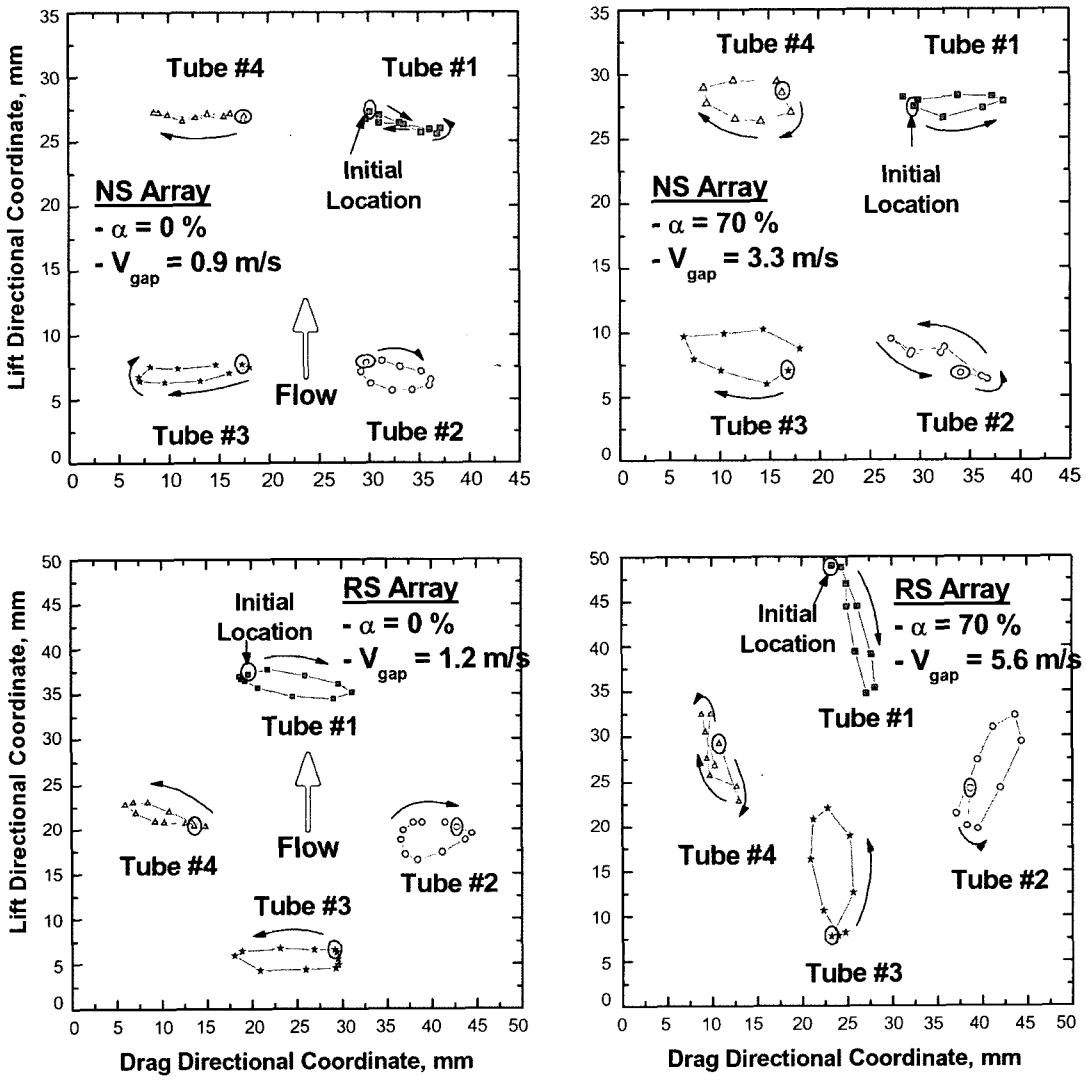

Fig. 7. Orbits of the Tube Vibration Motion in the NS Array and RS Array Tube Bundles for the Void Fraction of 0 % and 70 %

drag direction in the fluid-elastic instability region.

Beyond a void fraction of 80 %, the fluid-elastic instability condition was not reached due to the limited capacity of the air blower. However, as in the case of void fractions of 10 ~ 50 %, the maximum gap velocities supplied in the present RS array tests were much higher than the critical gap velocities of the present NS array tests for the same void fraction. That is, the maximum gap velocities of the RS array were 5.86, 5.93, and 6.11 m/s for void fractions of 80 %, 90 %, and 95 %, respectively. On the other hand, the critical gap velocities of the NS array were 2.35, 3.25, and 3.5 m/s for void fractions of 80 %, 90 %, and 95 %, respectively.

Figure 7 shows the representative orbits of the tube motion in the present NS array and RS array for void fractions of 0 % and 70 %. Each orbit corresponds to the critical gap velocity condition. The tube motion was evaluated from the high speed video recordings, which were taken at 1000 frames per second.

In the case of the NS array tube bundle, as generally recognized in the existing literature, the tubes vibrated mainly in the lift direction for a two-phase flow condition as well as a single-phase water flow condition. Also, the orbits of the RS array tube bundle in a single-phase water flow show the same trend wherein the lift directional tube motion overwhelmed the drag directional tube motion. On the contrary, the orbits of the RS array tube bundle in a two-phase flow condition conversely show that the tubes vibrated primarily in the drag direction, not in the lift direction.

Additional information of the phase relationship between neighboring tubes can be drawn from these orbits. In the case of the NS array tube bundle for a void fraction of 0 %, almost exactly 180 degrees of phase difference can be observed between the neighboring tubes in the lift direction, that is, between tube #1 and tube #4, and between tube #2 and tube #3. In addition, for a void fraction of 70 %, the tube motion between tube #1 and tube #4 shows a phase difference of about 180 degrees.

In the case of the RS array tube bundle for a void fraction of 0 %, a phase relationship of around 180 degrees can be seen between the tubes, that is, tubes #1 and #2, and tube #1 and tube #3. However, the phase relationship between the closest tubes, tubes #2 and #3, and tube #3 and tube #4 is not definitive but ambiguous. Instead, the tube motion between tube #1 and tube #3 shows a definitive phase relationship of 180 degrees. From the examination of these phase relationships, it can be qualitatively stated that a strong hydrodynamic coupling exists between neighboring tubes in the NS array tube bundle for both single -phase water flow and two-phase flow conditions. This can also be stated for the RS array tube bundle for a single-phase water flow condition. On the contrary, in the case of the RS array tube bundle for a two-phase flow condition, a strong hydrodynamic coupling exists between the tubes in the flow direction (tube #1 and tube #3), not between the neighboring tubes in the diagonal direction.

3.3 Damping

Damping ratio in a two-phase flow condition was measured for the in-flow condition using the rigid tube bundle. Power spectral density (PSD) functions for the drag and lift directions were obtained from 1,800 seconds records of the time domain vibration waveforms in the drag and lift directions. Total damping ratios for the drag and lift directions were evaluated using the following half power frequency bandwidth method. Figure 8 shows the typical PSD function obtained for the NS array tube bundle at a void fraction of 70 %.

$$\varsigma = \frac{f_2 - f_1}{f_n} \tag{6}$$

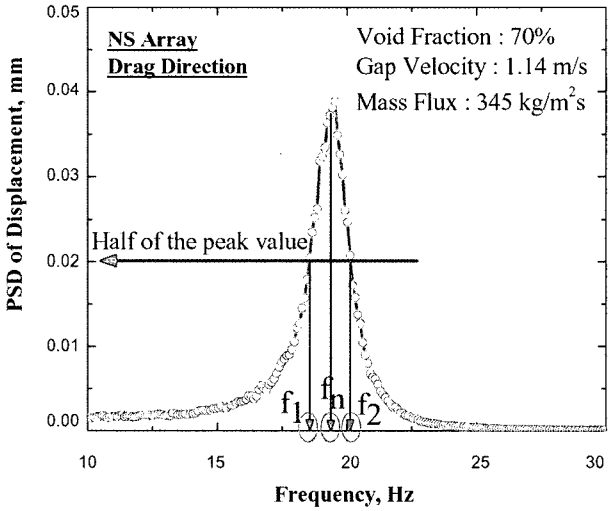

Fig. 8. Typical Power Spectral Density Function

Figures 9 and 10 present the total damping ratios, respectively, for the NS array and the RS array tube bundles, which were evaluated at various gap velocities and void fractions of 70 % and 90 %. The damping ratio was not sensitive to the gap velocity when the gap velocity was much lower than the critical gap velocity. As the gap velocity increased, the damping ratio showed a decreasing trend for the NS array tube bundle. However, the different results were observed for the RS array tube bundle. That is, the damping ratio was increased with increased gap velocity. The plateau region was approximately half the critical gap velocity for the NS array tube bundle, and approximately one-fourth the critical gap velocity for the RS array tube bundle.

In order to be consistent with the approach of Pettigrew et al. [1], the total damping ratio was evaluated at the gap velocity corresponding to the plateau region. As noted by Feenstra et al. [10], the original logic behind this approach is to avoid the fluid-elastic forces or hydrodynamic coupling, which would violate the assumption for the half power frequency bandwidth method.

Figure 11 shows the average total damping ratio obtained in the present NS and RS array tube bundles along with some existing data sets of Pettigrew et al. [1]. The average total damping ratio was obtained from the arithmetic mean of the total damping ratios for the drag and lift directions. The total damping ratio was strongly dependent on the void fraction, as noted by Pettigrew et al. [1], and it has a maximum value around 60~70% void fractions. In addition, the total damping ratio was not sensitive to the tube bundle arrangement such as the tube array type and p/d value.

3.4 Hydrodynamic Mass

Hydrodynamic mass was evaluated from the following equation suggested by Carlucci and Brown [13]:

$$m_h = m_t\left(\left(f_g / f\right)^2 - 1\right) \tag{7}$$

where m_t is the mass per unit length of the tube alone, and f_g and f are the tube frequencies in air and in a two-phase flow, respectively. The tube frequencies were obtained from the PSD functions, which were used for the damping ratio evaluation.

Figure 12 shows the measured hydrodynamic mass ratio in the present NS and RS array tube bundles together with some existing data sets of Pettigrew et al. [1], and it

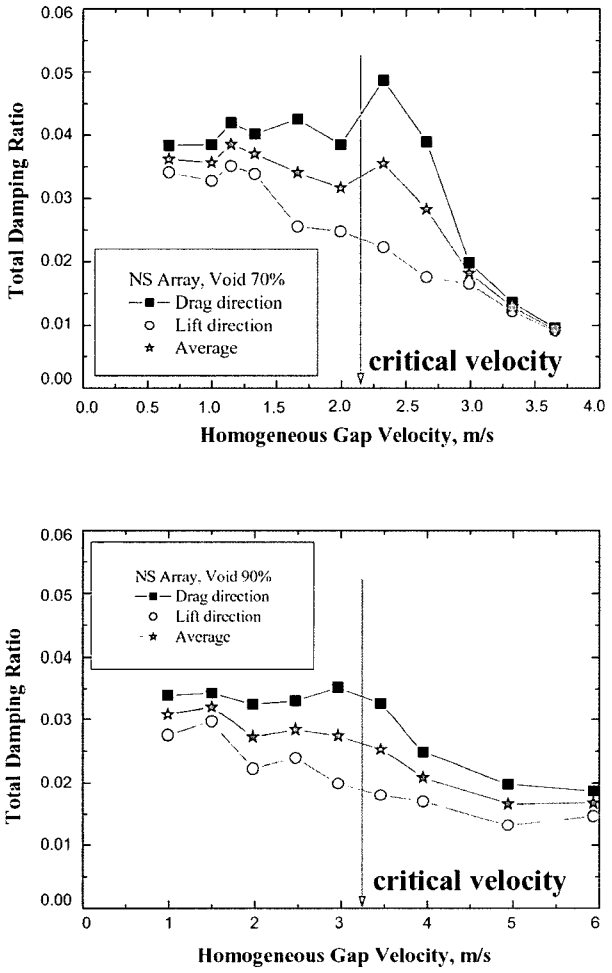

Fig. 9. Total Damping Ratio with Respect to the Gap Velocity in the NS Array Tube Bundle

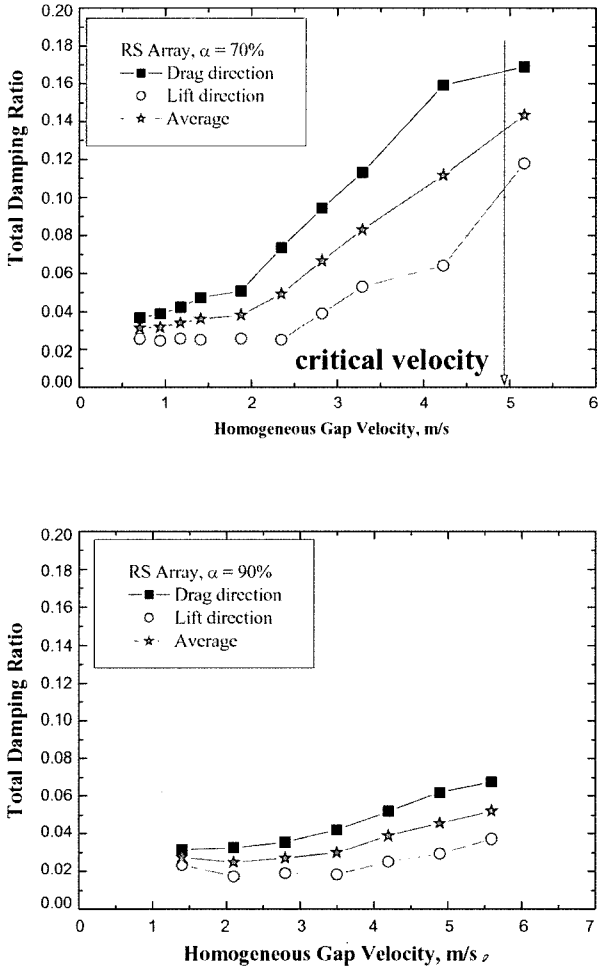

Fig. 10. Total Damping Ratio with Respect to the Gap Velocity in the RS Array Tube Bundle

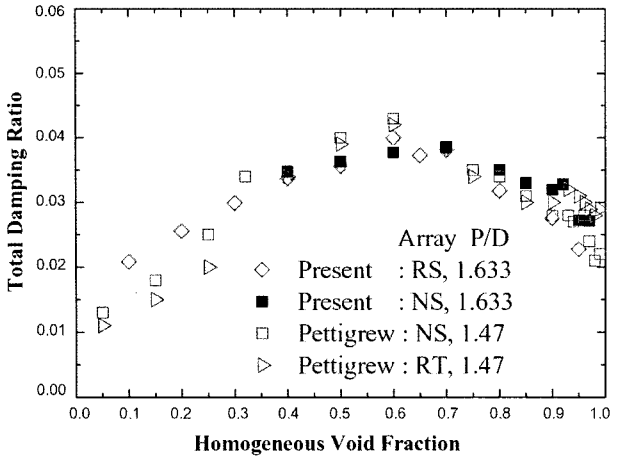

Fig. 11. Average Total Damping Ratio: the Present Data and the Existing Data

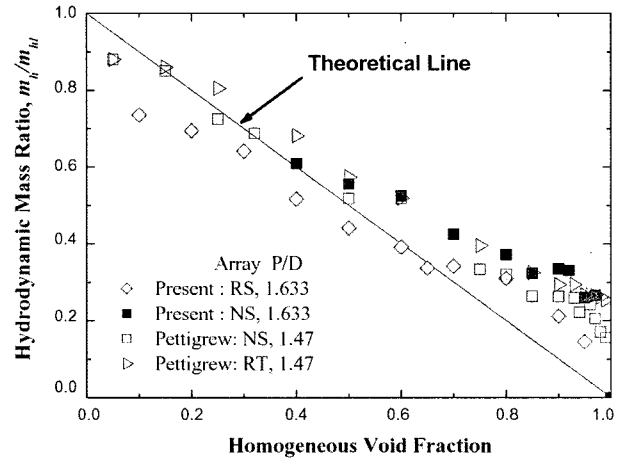

Fig. 12. Hydrodynamic Mass Ratio: Comparison of the Present Data with the Existing Data and Theoretical Values

compares the experimental data with the theoretically calculated values. Hydrodynamic mass ratio in Fig. 11 is defined as the ratio of the measured hydrodynamic mass in two-phase flow to the calculated hydrodynamic mass in a water flow from Eq. (8).

As in Pettigrew et al.'s work [1], hydrodynamic mass tends to have a higher value than the theoretical value above a void fraction of 80% regardless of tube bundle arrangement. They noted that this could be attributed to the intermittent flow, which has a greater liquid hold-up than a homogeneous mixture condition, and possibly a bubbly flow condition.

The hydrodynamic mass in the RS array tube bundle shows the lowest value among the data sets given in Fig. 12, which indicates a lower liquid hold-up around the tubes. This may have some relationship with the weak hydrodynamic coupling between the nearest neighboring tubes in the present RS array tube bundle for a two-phase flow condition.

Theoretical hydrodynamic mass in Fig. 12 was evaluated from the following equation presented in the work of Pettigrew et al. [1], and the original equation was derived by Rogers et al. [14]:

$$m_h = \left(\frac{\rho\pi d^2}{4}\right)\frac{(D_e/d)^2+1}{(D_e/d)^2-1} \tag{8}$$

where D_e is the equivalent diameter to model the confinement due to surrounding tubes. The following definition of D_e for the square tube array was presented by Pettigrew et al. [1].

$$D_e/d = (1.07 + 0.56\cdot p/d)\cdot p/d \tag{9}$$

3.5 Fluid-Elastic Instability

The most general method to predict the fluid-elastic instability would be Connors' relation, which can be formulated in terms of a dimensionless "reduced velocity" and a "mass damping parameter", as in the following equation:

$$\frac{V_{g,c}}{fD} = K\left(\frac{2\pi\zeta m}{\rho D^2}\right)^n \tag{10}$$

where $V_{g,c}$ is the critical gap velocity, f is the tube natural frequency in a fluid, ρ is the homogeneous mixture density, m is the mass per unit length (tube mass plus hydrodynamic mass), ζ is the total damping ratio, n is the exponent, and K is the instability factor. The instability factor (K) and the exponent of a mass damping parameter (n) should be obtained from the dimensionless "reduced velocity" and the "mass damping parameter".

Corresponding with the results of Pettigrew et al. [2], the present results obtained for the NS array tube bundle showed two regions of instability (Fig. 13). The first region corresponded to a lower void fraction region, and n and K had values of about 0.5 and 6.0, as could be predicted from Connors' relation for a single-phase flow. In the other region at a higher void fraction, n had a much lower value, less than 0.1. For this region, the critical flow velocities were much lower than predicted by Connors' relation of the former region. The transition between the two fluid-elastic instability regions occurred at a void fraction of approximately 90%, which corresponded to the flow regime transition from a bubbly flow to an intermittent flow.

In the case of the RS array tube bundle, the critical gap

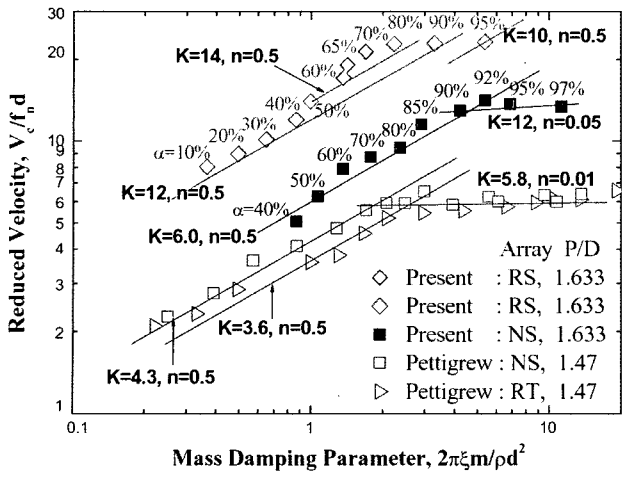

Fig. 13. Fluid-elastic Instability Results in Two-phase Cross-flow

velocity could be evaluated from the RMS tube displacement curves (Fig. 6) for void fractions of 60 ~ 70%. For this region, K of 14 and n of 0.5 were obtained. Even if the effect of the different array type is taken into consideration, a K value of 14 for the RS array is still much higher than the K value (i.e. 6) for the NS array.

For void fractions of 10 ~ 50 % and 80 ~ 95 %, the fluid -elastic instability was not observed for the maximum velocities supplied in the present experiments. However, a conservatively low value of K could be evaluated by assuming that the critical gap velocity was equal to the maximum supplied gap velocity, because the actual critical gap velocity would be higher than the maximum supplied gap velocity. All the conservative K values were higher than 12 except a K value of 10 for a void fraction of 95 %.

A summary of the present experimental results is provided in Table 1.

Table 1. Summary of the Experimental Results

Array	α (%)	f (Hz)	ζ_{total} (%)	ρ (kg/m³)	m_h (kg/m)	$V_{g,critical}$ (m/s)	$V_{g,max}$ (m/s)	Reduced Velocity	Mass Damping
NS	40	18.65	3.48	600.5	0.093	1.2		5.07	0.87
	50	18.85	3.63	500.7	0.085	1.5		6.27	1.06
	60	18.97	3.77	400.8	0.080	1.9		7.89	1.36
	70	19.37	3.85	300.9	0.065	2.15		8.74	1.78
	80	19.60	3.50	201.0	0.057	2.35		9.44	2.36
	85	19.81	3.30	151.1	0.050	2.9		11.53	2.90
	90	19.76	3.20	101.2	0.051	3.25		12.95	4.22
	92	19.78	3.28	81.1	0.051	3.53		14.12	5.38
	95	20.10	2.73	51.2	0.040	3.5		13.71	6.86
	97	20.07	2.71	31.2	0.041	3.4		13.40	11.25
RS	10	18.24	2.09	900.1	0.113		1.9	0.36	8.02
	20	18.38	2.55	801.1	0.107		2.14	0.49	8.96
	30	18.57	2.99	701.8	0.098		2.44	0.65	10.12
	40	19.05	3.37	600.6	0.079		2.9	0.86	11.99
	50	19.35	3.56	500.7	0.068		3.44	0.99	14.00
	60	19.56	4.00	400.9	0.060	4.24		1.36	17.08
	65	19.80	3.73	350.9	0.052	4.81		1.42	19.12
	70	19.78	3.81	301.0	0.052	5.37		1.69	21.40
	80	19.92	3.18	201.1	0.048		5.87	2.23	22.84
	90	20.38	2.76	101.2	0.033		5.93	3.30	22.92
	95	20.70	2.28	51.3	0.022		6.11	5.38	23.24

4. CONCLUDING REMARKS

Fluid-elastic instability characteristics in an air-water two-phase cross-flow have been experimentally investigated using two different arrays of straight tube bundles; NS array and RS array tube bundles with a p/d of 1.633.

The fluid-elastic instability for a two-phase flow condition occurred in the lift direction for the present NS array, as is in the previous results. However, it was found in the drag direction for the present RS array tube bundle. In addition, strong hydrodynamic coupling was observed between the neighboring tubes in the NS array tube bundle for a two-phase flow condition. On the contrary, in the case of the RS array tube bundle for a two-phase flow condition, strong hydrodynamic coupling was found between the tubes in the flow direction, not between the nearest neighboring tubes in the diagonal direction.

In the case of the RS array tube bundle, vortex shedding vibration excitation was observed in a two-phase flow condition up to a void fraction of 50 %, which was far beyond the range predicted from the previous experimental results.

The total damping ratio in each tube bundle was strongly dependent on the void fraction, and had a maximum at void fractions of 60~70%. Moreover, the damping ratio was not sensitive to the tube bundle array type. The hydrodynamic mass ratio in the RS array tube bundle had the lowest value among the data sets for various tube bundle configurations, which might be related to the weak hydrodynamic coupling in the RS array tube bundle.

The fluid-elastic instability in the NS array tube bundle showed two-regions of an instability, as in previous works. In addition, the transition between the two fluid-elastic instability regions was closely related to the flow regime transition. In the case of the RS array, a K value of 14 was obtained. The higher value of K for the RS array tube bundle is likely due to that a hydrodynamic coupling between the tubes in the flow direction is much higher than that between neighboring tubes in the diagonal direction.

Acknowledgments

The present work has been financially supported by the Ministry of Science and Technology (MOST) of the Korean government under the national nuclear mid- & long-term R&D program. The authors gratefully acknowledge helpful discussion with Dr. Won-Pil Baek at KAERI.

Nomenclature

$A\infty$	free stream flow area (m^2)
d	diameter of tube (m)
D_e	equivalent hydraulic diameter (m)
f	tube natural frequency in two-phase flow (Hz)
f_g	tube natural frequency in air (Hz)
K	instability constant of Connors' equation
m	total mass ($m_t + m_h$) per unit length (kg/m)
m_h	hydrodynamic mass per unit length (kg/m)
m_t	tube mass per unit length (kg/m)
n	exponent of mass damping parameter of Connors' equation
p	pitch of tube array (m)
Q	volumetric flow rate (m^3/s)
St	Strouhal number
$V\infty$	homogeneous free stream velocity (m/s)
V_g	homogeneous gap velocity (m/s)

Greek Letters

α	homogeneous void fraction
ζ	total damping ratio
ρ	homogeneous two-phase mixture density (kg/m^3)

Subscripts

l	liquid (or water) phase
g	gas (or air) phase
c	critical value

REFERENCES

[1] M. J. Pettigrew, C. E. Taylor, and B. S. Kim, "Vibration of Tube Bundles in Two-Phase Cross-Flow: Part 1–Hydrodynamic Mass and Damping," *Trans. ASME, J. Pressure Vessel Technology*, **111**, 466 (1989).

[2] M. J. Pettigrew, J. H. Tromp, C. E. Taylor, and B. S. Kim, "Vibration of Tube Bundles in Two-Phase Cross-Flow: Part 2–Fluid-Elastic Instability," *Trans. ASME, J. Pressure Vessel Technology*, **111**, 478 (1989).

[3] M. J. Pettigrew, C. E. Taylor, and B. S. Kim, "The Effects of Bundle Geometry on Heat Exchanger Tube Vibration in Two-Phase Cross Flow," *Trans. ASME, J. Pressure Vessel Technology*, **123**, 414 (2001).

[4] M. J. Pettigrew, C. E. Taylor, J. H. Jong, and I. G. Currie, "Vibration of a Tube Bundle in Two-Phase Freon Cross-Flow," *Trans. ASME, J. Pressure Vessel Technology*, **117**, 321 (1995).

[5] C. E. Taylor, I. G. Currie, M. J. Pettigrew, and B. S. Kim, "Vibration of Tube Bundles in Two-Phase Cross-Flow: Part 3 – Turbulence-Induced Excitation," *Trans. ASME, J. Pressure Vessel Technology*, **111**, 488 (1989).

[6] F. Axisa, M. Wullschleger, B. Villard, and C. Taylor, "Flow -Induced Vibration of Steam Generator Tubes," EPRI Report: EPRI NP-4559 (1986).

[7] T. Nakamura, K. Fujita, K. Kawanishi, N. Yamaguchi, and A. Tsuge., "Study on the Vibrational Characteristics of a Tube Array Caused by Two-Phase Flow. Part II: Fluidelastic Vibration," *J. Fluids and Structures*, **9**, 539 (1995).

[8] K. Hirota, T. Nakamura, N. Mureithi, T. Ueno, and K. Tomomatsu, "Dynamics of an Inline Tube Array in HCFC-123 Two-Phase Flow (Comparison with Steam-Water Two-Phase Flow)," *Proc. of ASME Winter Annual Meeting*, AD-Vol 53-2 (1997).

[9] P. A. Feenstra, R. L. Judd, and D. S. Weaver, "Fluidelastic Instability in a Tube Array Subjected to Two-Phase R-11 Cross-Flow, *J. Fluids and Structures*, **9**, 747 (1995).

[10] P. A. Feenstra, D. S. Weaver, and T. Nakamura, "Vortex Shedding and Fluidelastic Instability in a Normal Square

Tube Array Excited by Two-Phase Cross-Flow," *J. Fluids and Structures*, **17**, 793 (2003).
[11] I. C. Chu, H. J. Chung, B. M. Bae, and Y. J. Yun, "The Effect of the Flow Regime Transition on the Fluid-Elastic Instability," *Trans. KPVP*, **1**, 1 (2005).
[12] R. Ulbrich and D. Mewes, "Vertical, Upward Gas-Liquid Two-Phase Flow Across a Tube Bundle," *Int. J. Multi. Flow*, **20**, 249 (1994).
[13] L. N. Carlucci and J. D. Brown, "Experimental Studies of Damping and Hydrodynamic Mass of a Cylinder in Confined Two-Phase Flow" *Trans. ASME, J. Vibration, Stress and Reliability in Design*, **105**, 83 (1983).
[14] R. G. Rogers, C. E. Taylor, and M. J. Pettigrew, "Fluid Effects on Multispan Heat Exchanger Tube," *ASME PVP Conf.*, San Antonio, Texas, USA (1984).